34th AIAA Fluid Dynamics Conference and Exhibit
28 June - 1 July 2004, Portland, Oregon

AIAA 2004-2548

Large Eddy Simulation Using an Unstrcutured Mesh Based Finite-Volume Solver

Sung-Eun Kim*
Fluent Inc., Lebanon, NH 03766

This paper concerns development of a large eddy simulation (LES) capability for a finite-volume solver which permits use of unstrcutured meshes. The solver employs a cell-centered scheme based on a multi-dimensional linear reconstruction scheme. Both convection and diffusion terms are discretized using central-differencing scheme. A three-level, second-order scheme is used for temporal discretization. For subgrid-scale turbulence modeling, the dynamic Smagorinsky's model and the dynamic turbulent kinetic energy transport model were implemented. A noble test-filter was designed which is applicable to unstructured meshes of arbitrary cell topology. The dynamic procedure is local, which renders itself applicable to three-dimensional flows without any homogenous directions. The wall boundary condition is effected using a wall-function approach which applies appropriate wall-laws depending on the near-wall mesh resolution. The LES capability is validated for several wall-bounded flows including a fully-developed channel flow, a cavity flow, flow around a sqaure cylinder, flow around a sphere. The results are in good agreements with the data and the numerical results reported by others.

Introduction

We encounter, with an increasing frequency, industrial applications of computational fluid dynamics (CFD) where the turbulent flows in question are dominated by unsteady large-scale coherent structures. Those large-scale structures greatly impact various important aspects of the flow devices or systems in question such as energy consumption, safety, and noise. The ramification of whether or not one can predict and harness their behaviors and their consequences is therefore quite significant. Attempts to predict these flows using unsteady RANS (URANS) equations, even with todays' most advanced turbulence model, have been met with limited success.

Large eddy simulation (LES) is better suited for the task, for it is designed to directly resolve large-scale structures with only the effects of smaller sub-grid scales on the resolved scales accounted for via turbulence modeling. The main obstacle is the prohibitive amount of computational resource and effort incurred by large number of computational elements, which translates into large memory requirement and unduly long solution turnaround time. Nonetheless, being encouraged by today's computing power, a growing number of industrial CFD practitioners have come to perceive LES as a feasible, if not yet fully practical, approach to modeling industrial turbulent flows.

This paper is concerned with development of a LES capability in a finite-volume solver[1–4] which permits use of unstructured meshes. The LES capability can therefore handle complex geometries frequently encountered in industrial applications, which will greatly benefit industrial applications. Two contemporary subgrid-scale turbulence models were implemented, including the dynamic Smagorinsky's model[5,6] and the dynamic subgrid-scale turbulence kinetic energy model.[7]

We will start with a brief description of the subgrid-scale turbulence models adopted in this study along with the details of the implementation such as the test-filter designed with its applicability for arbitrary unstructured meshes in mind. This will be followed by an overview of the numerics and the validation studies for a number of simple to moderately complex flows.

Filtered Navier-Stokes Equations

The governing equations for LES are obtained by filtering the Navier-Stokes equations in either Fourier (wavenumber) space or physical space. In this process, the eddies smaller than the filter width or grid spacing used in the computations are filtered out. The resulting equations thus govern the dynamics of the large eddies.

A filtered variable (denoted by an overbar) is defined by;

$$\overline{\phi}(\mathbf{x}) = \int_{\mathcal{D}} \phi(\mathbf{y}) G(\mathbf{x},\mathbf{y}) d\mathbf{y} \tag{1}$$

where $\mathcal{D}$ is the computational domain, $\mathbf{y} \in \mathcal{D}$ and G is the filter function that determines the size of the resolved scales.

In the finite-volume discretization employed here, the discrete solution is defined as

$$\overline{\phi}(\mathbf{x}) = \frac{1}{V}\int_{\mathcal{V}} \phi(\mathbf{y})\,\mathbf{dy}, \quad \mathbf{y} \in \mathcal{V} \tag{2}$$

where V is the volume of a computational cell.

The definition in eq. (2) of the discrete solution variables can be viewed as a filtering operation. The implied filter function, $G(\mathbf{x},\mathbf{y})$, is thus a top-hat filter given by

$$G(\mathbf{x},\mathbf{y}) = \begin{cases} 1/V & \text{for } |\mathbf{x}-\mathbf{y}| \in \mathcal{V} \\ 0 & \text{otherwise} \end{cases} \tag{3}$$

*Principal Engineer, Turbulence and Acoustics Modeling Group; sek@fluent.com, Member AIAA.

We can write the filtered Navier-Stokes equations for incompressible flows (for the sake of conciseness) as

$$\frac{\partial \overline{u}_i}{\partial t} + \frac{\partial \overline{u}_i \overline{u}_j}{\partial x_j} = -\frac{1}{\rho}\frac{\partial \overline{p}}{\partial x_i} - \frac{\partial \tau_{ij}}{\partial x_j} + \frac{\partial}{\partial x_j}\left(\nu \frac{\partial \overline{u}_i}{\partial x_j}\right) \quad (4)$$

$$\frac{\partial \overline{u}_i}{\partial x_i} = 0 \quad (5)$$

where τ_{ij} is the subgrid-scale stress defined by;

$$\tau_{ij} \equiv \overline{u_i u_j} - \overline{u}_i \overline{u}_j \quad (6)$$

Subgrid-Scale Turbulent Stress Models

The subgrid-scale(SGS herefrom) turbulent stress resulting from the filtering operation in eq. (6) is unknown, and need a closure.

The models based on isotropic eddy-viscosity computes SGS stresses from

$$\tau_{ij} - \frac{1}{3}\tau_{kk}\delta_{ij} = -2\nu_t \overline{S}_{ij} \quad (7)$$

where ν_t is the SGS eddy-viscosity, and $\overline{S}_{ij}$ is the resolved rate-of-strain tensor defined by;

$$\overline{S}_{ij} \equiv \frac{1}{2}\left(\frac{\partial \overline{u}_i}{\partial x_j} + \frac{\partial \overline{u}_j}{\partial x_i}\right)$$

The task now is to determine the SGS viscosity, ν_t .

Smagorinsky's Model

In this simple model proposed by Smagorinsky,[5] the SGS eddy-viscosity is computed using:

$$\nu_t = C_\nu \overline{\Delta}^2 \left|\overline{S}\right| \quad (8)$$

where C_ν is a model constant, $\left|\overline{S}\right| \equiv \sqrt{2\overline{S}_{ij}\overline{S}_{ij}}$ the modulus of rate-of-strain for the resolved scales, and $\overline{\Delta}$ is the grid-filter length (or width) computed from

$$\overline{\Delta} = V^{1/3} \quad (9)$$

The subgrid-scale stress is consequently,

$$\tau_{ij} - \frac{\delta_{ij}}{3}\tau_{kk} = -2C_\nu \overline{\Delta}^2 \left|\overline{S}\right| \overline{S}_{ij} \quad (10)$$

This model boasts its simplicity, economy, and robustness. Notwithstanding these merits, this model has also several well-known shortcomings. The most problematic aspect of the model from a practical standpoint is that there is no single value of the model constant (C_ν) which is universally applicable to a wide range of flows.

Dynamic Smagorinsky Model (DSM)

Germano *et al.*[14] and subsequently Lilly[6] conceived a procedure in which the model constant, C_ν, is dynamically computed based on the information provided by the resolved scales of motion. The dynamic procedure thus obviates the need for computors to specify the model constant in advance. The dynamic procedure requires the so-called "test" filter ($\widetilde{\Delta}$) which is needed to obtain the small scales of the resolved field. Denoting the test-filtered quantities by a *tilde*, we can write the test-filtered Navier-Stokes equations as

$$\frac{\partial \widetilde{\overline{u}}_i}{\partial t} + \frac{\partial \widetilde{\overline{u}}_i \widetilde{\overline{u}}_j}{\partial x_j} = \frac{1}{\rho}\frac{\partial \widetilde{\overline{p}}}{\partial x_i} - \frac{\partial T_{ij}}{\partial x_j} + \frac{\partial}{\partial x_j}\left(\nu \frac{\partial \widetilde{\overline{u}}_i}{\partial x_j}\right) \quad (11)$$

$$\frac{\partial \widetilde{\overline{u}}_i}{\partial x_i} = 0 \quad (12)$$

where T_{ij} is now a "subtest-scale" stress defined by;

$$T_{ij} \equiv \widetilde{\overline{u_i u_j}} - \widetilde{\overline{u}}_i \widetilde{\overline{u}}_j \quad (13)$$

Central to the dynamic modeling is the similarity concept that T_{ij} is associated with larger scales, yet is dynamically similar to τ_{ij}, and therefore can be modeled using the same parameterization as the one used for τ_{ij},[14] which leads to

$$T_{ij} - \frac{\delta_{ij}}{3}T_{kk} = -2C_\nu \widetilde{\Delta}^2 \left|\widetilde{\overline{S}}\right| \widetilde{\overline{S}}_{ij} \quad (14)$$

where $\widetilde{\Delta}$ is the test-filter width. Note that the same model coefficient, C_ν, is used in the modeling of both τ_{ij} and T_{ij}.

τ_{ij} and T_{ij} are related to each other by

$$\begin{aligned} T_{ij} - \widetilde{\tau}_{ij} &= \widetilde{\overline{u_i u_j}} - \widetilde{\overline{u}}_i \widetilde{\overline{u}}_j - \left(\widetilde{\overline{u_i u_j}} - \widetilde{\overline{u_i}}\,\widetilde{\overline{u_j}}\right) \\ &= \widetilde{\overline{u_i}}\,\widetilde{\overline{u_j}} - \widetilde{\overline{u}}_i \widetilde{\overline{u}}_j \equiv L_{ij} \end{aligned} \quad (15)$$

The stress components, L_{ij}, can be interpreted as the stress associated with the smallest resolved scales between the test-filter scale ($\widetilde{\Delta}$) and the grid-filter scale ($\overline{\Delta}$). Since L_{ij} can be directly computed from the resolved scales, the identity given by eq. (15) can be used to determine the model constant. Thus, we have

$$L_{ij} - \frac{\delta_{ij}}{3}L_{kk} = \alpha_{ij} C_\nu - \widetilde{\beta_{ij} C_\nu} \quad (16)$$

where

$$\alpha_{ij} = -2\widetilde{\Delta}^2 \left|\widetilde{\overline{S}}\right| \widetilde{\overline{S}}_{ij} \quad (17)$$

$$\beta_{ij} = -2\overline{\Delta}^2 \left|\overline{S}\right| \overline{S}_{ij} \quad (18)$$

Note that C_ν is under the test-filtering operator. As often done to simplify the procedure, C_ν is taken out from the test-filter operation as,

$$L_{ij} - \frac{\delta_{ij}}{3}L_{kk} = C_\nu \left(\alpha_{ij} - \widetilde{\beta_{ij}}\right) \quad (19)$$

eq. (26) is an overdetermined system of equation, since there are more equations than the single unknown, C_ν. Following Lilly's idea,[6] the model constant C_ν is obtained by seeking forC_ν which minimizes the square of the error defined as:

$$E = \left(L_{ij} - \frac{\delta_{ij}}{3} L_{kk} - C_\nu M_{ij} \right)^2 \tag{20}$$

where

$$M_{ij} \equiv \alpha_{ij} - \widetilde{\beta_{ij}} = -2 \left(\widetilde{\Delta}^2 \left| \widetilde{\overline{S}} \right| \widetilde{\overline{S}}_{ij} - \overline{\Delta}^2 \widetilde{|\overline{S}|\overline{S}_{ij}} \right)$$

Taking $\partial E / \partial C_\nu$ and setting it zero, we obtain

$$C_\nu = \frac{L_{ij} M_{ij}}{M_{ij} M_{ij}} \tag{21}$$

The model constant, C_ν, thus obtained is a local value, varying in time and space in a fairly wide range, both negative and positive. Although a negative C_ν and consequently negative eddy-viscosity is often interpreted as the flow of energy from the subgrid-scale eddies to the resolved eddies (referred to as "back-scatter") and regarded as a desirable attribute of the dynamic models, too large a negative eddy-viscosity causes numerical instability, ultimately leading to an excessive level of numerical noise or even divergence of the numerical solution. To avoid this, we simply clip C_ν at zero. This is slightly different from the usual practice in which the total viscosity (laminar viscosity + eddy-viscosity) is clipped, thus allowing a small SGS eddy-viscosity.

Dynamic Subgrid Kinetic Energy Model (DKEM)

The original and dynamic Smagorinsky's model discussed so far are essentially algebraic models in which subgrid-scale stresses are parametrized using the resolved velocity scales. The underlying assumption is the local equilibrium between the transferred energy through the grid-filter scale and the dissipation of kinetic energy at small subgrid scales. The subgrid-scale turbulence can be represented more faithfully by account for the transport of the subgrid-scale turbulent kinetic energy. To this end, we chose to use the model of Kim and Menon.[7] This SGS turbulent kinetic energy transport model accounts for the history and non-local effects, having the potential to benefit complex flows with non-equilibrium turbulence.

The SGS kinetic energy is defined as

$$k_{sgs} = \frac{1}{2} \left(\overline{u_k^2} - \overline{u}_k^2 \right) \tag{22}$$

which is obtained by contracting the subgrid-scale stress in eq. (6).

The subgrid-scale eddy viscosity, ν_t, is computed using k_{sgs} as

$$\nu_t = C_k k_{sgs}^{1/2} \overline{\Delta} \tag{23}$$

The subgrid-scale stress can then be written as

$$\tau_{ij} - \frac{2}{3} k_{sgs} \delta_{ij} = -2 C_k k_{sgs}^{1/2} \overline{\Delta} \overline{S}_{ij} \tag{24}$$

k_{sgs} is obtained by solving its transport equation

$$\frac{\partial \overline{k}_{sgs}}{\partial t} + \frac{\partial \overline{u}_j \overline{k}_{sgs}}{\partial x_j} = -\tau_{ij} \frac{\partial \overline{u}_i}{\partial x_j} - C_\varepsilon \frac{k_{sgs}^{3/2}}{\overline{\Delta}} + \frac{\partial}{\partial x_j} \left(\frac{\nu_t}{\sigma_k} \frac{\partial k_{sgs}}{\partial x_j} \right) \tag{25}$$

There are three model constants appearing in this equation, namely, C_k, C_ε, and σ_k, which need to be specified. These "user-adjustable" constants shares the same predicament as the Smagorinsky's model in that one has to specify the values.

Kim and Menon[7] proposed a dynamic procedure which is similar to the one for the Smagorinsky'd model described earlier. However, there is a subtle but significant difference between the two dynamic procedures. The dynamic procedure of Kim and Menon is based on the hypothesis that there is a significant correlation between the subgrid scale stress, τ_{ij}, and the subtest-scale Leonard stress, L_{ij}, as corroborated by the experimental data reported by Liu *et al.*[18,19] Thus, L_{ij} is parametrized by

$$L_{ij} - \frac{\delta_{ij}}{3} L_{kk} = -2 C_k \widetilde{\Delta} k_{test}^{1/2} \widetilde{\overline{S}}_{ij} \tag{26}$$

where k_{test} is the resolved kinetic energy associated with the scales between the test-filter and the grid-filter, defined as

$$k_{test} = \frac{1}{2} \left(\widetilde{\overline{u_k} \overline{u_k}} - \widetilde{\overline{u}}_k \widetilde{\overline{u}}_k \right) \tag{27}$$

It should be noted that DSM applies the similarity argument to the resolved stress, L_{ij}, directly without having to invoke Germano's identity. Unlike the corresponding equation in DSM, eq. (26) does not involve any test-filter operation on C_k. C_k appearing in eq. (26) is an indisputably local quantity which can be readily computed by minimizing the least-square error as in the DSM. The rest of the procedure remains exactly the same as before except the new definition of M_{ij}

$$M_{ij} \equiv -2 \widetilde{\Delta}^2 \left| \widetilde{\overline{S}} \right| \widetilde{\overline{S}}_{ij} \tag{28}$$

DKEM has several desirable attributes which alleviate the difficulties in using DSM. First, DSM is self-consistent in that the procedure does not involve the filtering operation of the model coefficient, C_ν. Secondly, the ill-conditioned denominator in the expression for C_ν in DSM, which can become very small in a considerable fraction of the domain, is now replaced with much more benign one than in DSM. Lastly, once can save a small amount of computational effort, since the test-filtering operation on SGS stress (β_{ij}) is not needed.

As a consequence, we can compute the model constant C_k from

$$C_\nu = \frac{\widetilde{L_{ij}L_{ij}}}{M_{ij}M_{ij}} \tag{29}$$

where M_{ij} is defined by

$$M_{ij} = -2\tilde{\Delta}k_{test}^{1/2}\widetilde{\overline{S}}_{ij} \tag{30}$$

The model constant, C_ε can also be determined by a dynamic procedure. It is assumed that the dissipation of k_{test} can be modeled similar to the dissipation of subgrid-scale kinetic energy.

$$e = C_\varepsilon \frac{k_{test}^{3/2}}{\tilde{\Delta}} \tag{31}$$

Now we can see that the dissipation of the subtest-scale kinetic energy can also be computed from

$$e = (\nu + \nu_t)\left(\widetilde{\frac{\partial\overline{u_i}}{\partial x_j}\frac{\partial\overline{u_i}}{\partial x_j}} - \frac{\partial\widetilde{\overline{u}}_i}{\partial x_j}\frac{\partial\widetilde{\overline{u}}_i}{\partial x_j}\right) \tag{32}$$

The model constant, C_ε, can be obtained from eq. (31) and eq. (32).

$$C_\varepsilon = \frac{\tilde{\Delta}(\nu+\nu_t)}{k_{test}^{3/2}}\left(\widetilde{\frac{\partial\overline{u_i}}{\partial x_j}\frac{\partial\overline{u_i}}{\partial x_j}} - \frac{\partial\widetilde{\overline{u}}_i}{\partial x_j}\frac{\partial\widetilde{\overline{u}}_i}{\partial x_j}\right) \tag{33}$$

The Prandtl number, σ_k can also be obtained from a dynamic procedure. However we decided to not to do this and instead to take the constant value ($\sigma_k = 1.0$)

Choice of test-filter

The dynamic procedure described in the foregoing requires the test-filter. One criterion in choosing the test-filter is that the test-filter ought to be consistent with the grid-filter. To meet this requirement, we should adopt a top-hat filter whose properties remain the same as those of the grid-filter. In addition, the test-filter should be applicable to unstructured meshes. Among many alternatives we have tried so far, the most straightforward one seems to be the top-hat filter involving the computational elements (cells) neighboring the cell under consideration. The neighboring cells for the test filter are shown in Figure 1 as the shaded cells.

$$\widetilde{\overline{\phi}}(c_0) = \frac{1}{\sum_n V_i}\int_{V_{tot}} \overline{\phi}\, d\mathcal{V} = \frac{\sum_i \overline{\phi}_i V_i}{\sum_i V_i} \tag{34}$$

Flow solvers

FLUENT offers both *segregated* solver and *coupled* solvers. These two solvers employ different solution algorithms yet share several key features such as cell-centered finite-volume discretization and multi-dimensional linear reconstruction scheme. They allow use of computational elements (cells) with arbitrary polyhedral topology, including

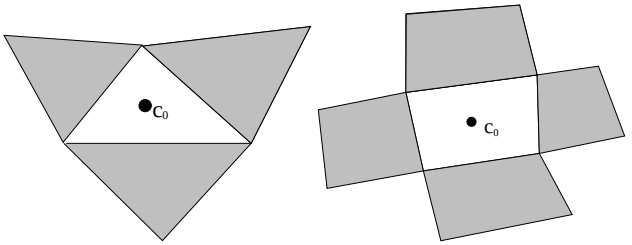

Fig. 1 Computational cells involved in test-filter operation, left:triangular mesh ; right: quadrilateral mesh

quadrilateral, hexahedral, triangular, tetrahedral, pyramidal, prismatic, and hybrid meshes. The two solvers also share the same suite of turbulence models such as eddy-viscosity transport model, a family of $k-\varepsilon$ models, $k-\omega$ models, and Reynolds-stress transport model (RSTM).

In the segregated solver, convection terms are discretized using a second-order upwind scheme or a central-differencing scheme, and diffusion terms a central differencing scheme. The governing equations are solved in a sequential (segregated) manner. The discretized algebraic equations are solved using a point-wise Gauss-Seidel iterative algorithm. Algebraic multi-grid (AMG) method is employed to accelerate solution convergence. For temporal discretization, the segregated solver uses a three-level, second-order scheme. The overall time-advancement algorithm is based on a generalized fractional-step method. The splitting error can be driven to zero if the sub-iterations are carried out per time-step.

The coupled solver[3,4] solves Euler, Navier-Stokes, or Reynolds-averaged Navier-Stokes equations in a coupled manner. The time-derivative preconditioning of the governing equations adopted in the coupled solver allows the solutions of both compressible and incompressible flows. The coupled solver employs a second-order upwind flux-difference splitting (FDS) scheme for convection terms and a central differencing scheme for diffusion terms. The resulting (coupled) system of discretized equations is then solved for the primitive variables using an Algebraic Multigrid (AMG) algorithm, with the point Gauss-Seidel relaxation as a smoother. The CPU usage in the coupled solver scales linearly with the number of cells used.

Validation of numerics

Here we present a validation for a laminar transient flow to establish the formal order of both spatial and temporal discretization accuracy. The problem considered is what is often referred to as Taylor's vortex which represents a periodic array of counter-rotating vortices decaying with time. This flow has an analytical solution, being frequently used to verify numerical accuracy

$$u = -\cos x \sin y\, e^{-2t/Re} \tag{35}$$

$$v = \sin x \cos y \, e^{-2t/Re} \quad (36)$$

$$p = -0.25(\cos 2x + \cos 2y) \, e^{-4t/Re} \quad (37)$$

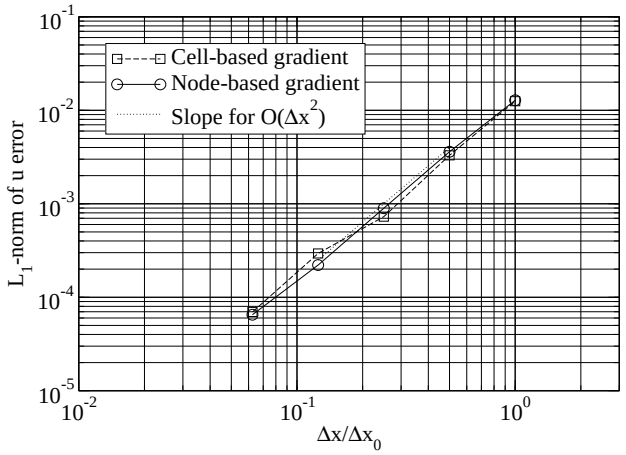

Fig. 2 L_1 norm of spatial error for u computed at $t = 32$ for the decaying vortex (Taylor's) problem

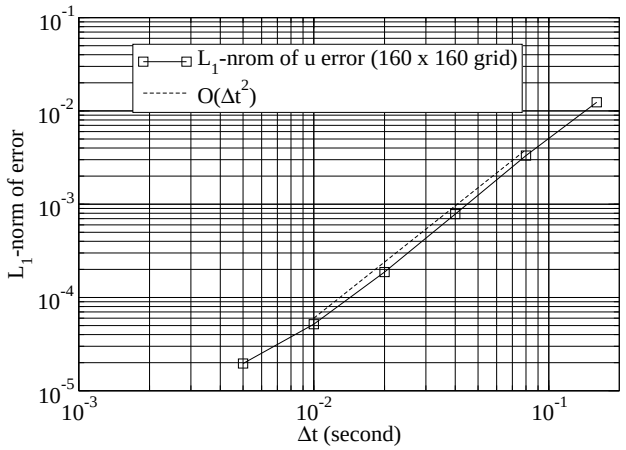

Fig. 3 The Variation of L_1-norm of temporal error for u with δt - computed at $t = 32$ for the decaying vortex (Taylor's) problem

To ascertain the spatial accuracy, the computations were made first using five different triangular meshes which were progressively refined.

Figure 2 shows the error for the x-velocity component in terms of L_1 norm, defined by

$$L_1 = \frac{1}{N}\sum_{1}^{N} |u_{exact} - u|$$

. Figure 3 shows the error as the temporal resolution, namely, time-step, is refined. We used here the finest mesh (160×160 cells). It clearly shows that our time-advancement scheme is has a second-order accuracy.

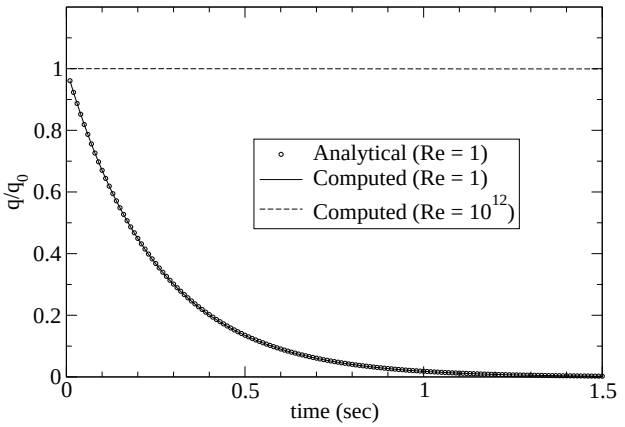

Fig. 4 Evolution of the total kinetic energy with time for the decaying vortex (Taylor's) problem

In addition, we computed this flow with the inviscid fluid to demonstrate that the discretization schemes employed here are non-diffusive and preserve the kinetic energy. Figure 4 shows the time evolution of the total kinetic energy (summed over the domain) which were predicted using two different fluid viscosities.

LES Validations

The validation studies have been carried out for a number of wall-bounded flows which range from a fully developed channel flows to flows around bluff bodies. The preliminary results are discussed below.

Fully-developed channel flow

The computations have been carried out for the Reynolds number of Re_τ = 395. The computational domain corresponds to a box $[2\pi H \times 2H \times \pi H]$ in the axial, normal, and transverse directions, respectively. A hexahedral mesh with $72 \times 72 \times 72$ cells was used for the computations. The mesh is such that the distance at the first wall-adjacent cell is approximately $7 \times 10^{-4}\, H$ translates to $y+ \approx 0.3$. A physical time-step corresponding to $\Delta t^+ = 1.0$ was used.

The mean velocity and the r.m.s. velocity components predicted using the DSM are shown in Figure 5 and Figure 6, respectively. Noticeably, the spatial homogeneity of the time-averaged quantities is not completely achieved yet as indicated by the spanwise variation of the profiles. Nonetheless, the predictions are overall fairly good. The computation is still undergoing to attain the statistically stationary state. In the full paper, comparisons will be made between the results from the DSM and DKEM models. The full paper will also address the issue of mesh dependency of the predictions.

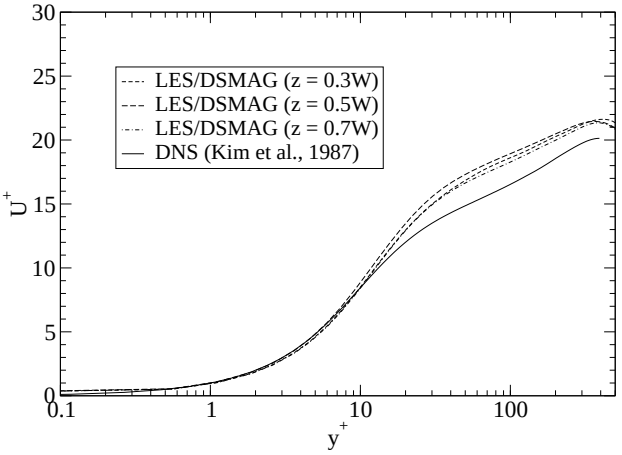

Fig. 5 Time-averaged axial velocity distributions at several spanwise locations - predicted by the dynamic Smagorinsky's (DSM) SGS viscosity model

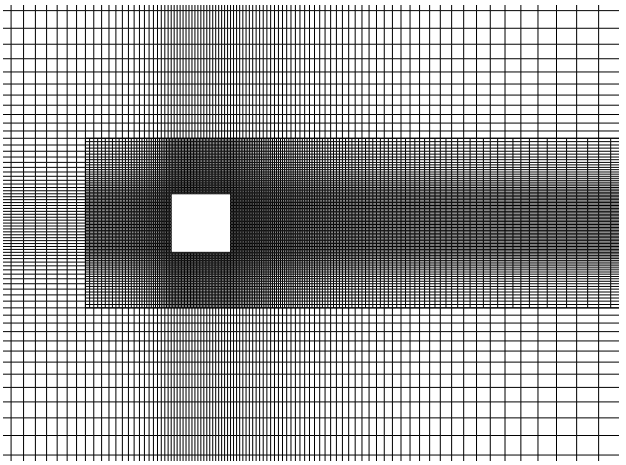

Fig. 7 A longitudinal cut of the mesh used in LES for the sqaure cylinder

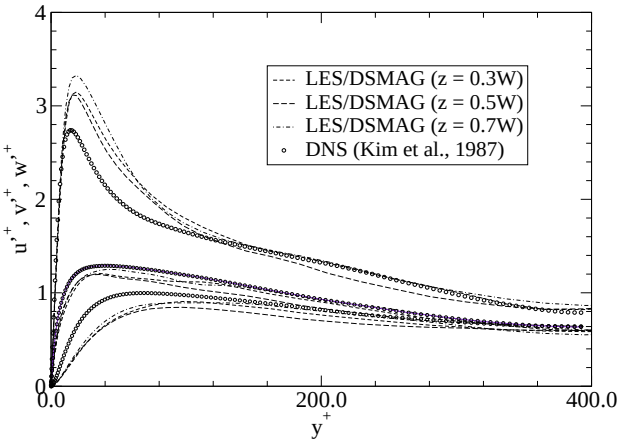

Fig. 6 The r.m.s. velocity distributions at several spanwise locations - predicted by the dynamic Smagorinsky's (DSM) SGS viscosity model

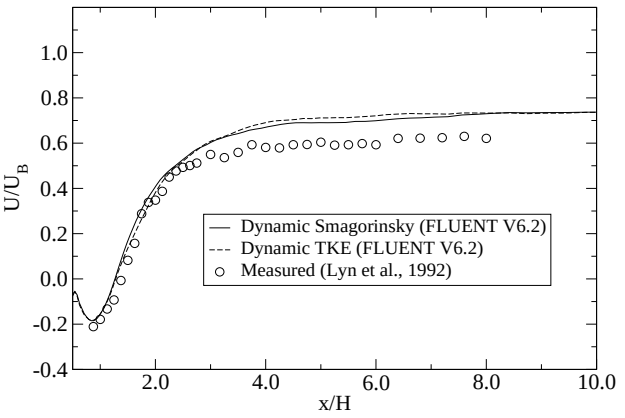

Fig. 8 Time-averaged axial velocity distributions in the wake predicted by DSM and DKEM

Vortex-shedding behind a square cylinder

The flow past a square cylinder studied experimentally by Lyn *et al.*[25] has been considered. The Reynolds number based on the freestream velocity (U_0) and the width of the cylinder (W) is 21,000. Several others have also computed this flow using LES.[24] The mesh used for the present computation is a hexahedral mesh with a total of 660,000 elements. As shown in the figure, the mesh has an embedded region of fine mesh designed to enhance the mesh resolution near the cylinder without incurring too large an increase in the total number of the computational elements.

Figure 8 shows the time-averaged axial velocity profiles in the wake which were predicted using the two dynamic SGS viscosity models. The predicted axial velocity distributions are seen to reach asymptotically $0.75\ U_0$, which is substantially lower than what the experimental data indicates ($0.62\ U_0$). Interestingly, this overprediction of the mean velocity in the wake has been also found in several other computations.[?] Figure 9 depicts the r.m.s. axial velocity (u'/U_0) distributions recorded at several different spanwise locations in the wake. Despite the lack of the spatial homogeneity, the results are quite encouraging.

The full paper will address the mesh-dependency of the predictions using the results for one coarse mesh mesh and one fine mesh, for which the computations are under way. In the full paper, the computational results will be compared with the experimental data in terms of the forces acting on

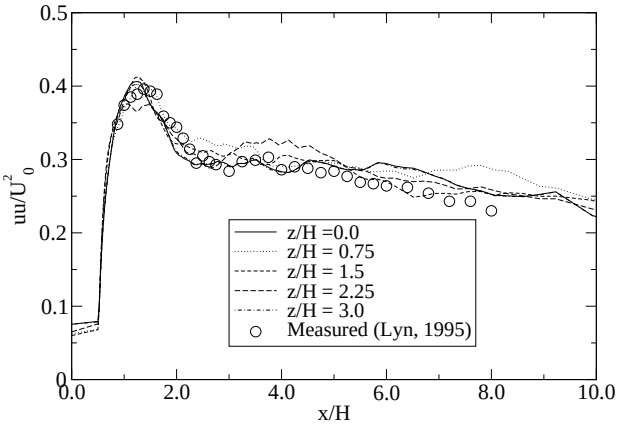

Fig. 9 The r.m.s. axial velocity fluctuation in the wake of a square cylinder predicted by the DSM - sampled at several spanwise locations

the cylinder, the mean velocity and turbulence fields in the near-wake.

Flow around a sphere

We considered the flow around a sphere at the Reynolds number(Re_D) of 10,000. This flow is more challenging, since the body does not have any salient edge as in the case of the square cylinder.

The computation is under way using a tetrahedral mesh and a hexahedral mesh. The results from these computations will give us an opportunity to assess the fidelity of LES on unstructured meshes.

7. Summary and conclusion

To be completed in the full paper

Acknowledgments

The author acknowledges use of Fluent Inc.'s software and thank the members of the product development group at Fluent Inc.

References

[1] Mathur, S. R. and Murthy, J. Y.,"A Pressure-Based Method for Unstructured Meshes," *Numerical Heat Transfer*, vol. 31, pp. 195-215, 1997.

[2] Kim, S.-E., Mathur, S. R., Murthy, J. Y., and Choudhury, D., "A Reynolds-Averaged Navier-Stokes Solver Using Unstructured Mesh-Based Finite-Volume Scheme," AIAA-Paper 98-0231, 1998.

[3] Smith, W.A. and Weiss, J.M., Preconditioning Applied to Variable and Constant Density Flows, *AIAA J.* Vol. 33, No. 11, November 1995.

[4] Weiss, J.M., Maruszewski, J.P. and Smith, W.A., Implicit Solution of the Navier-Stokes Equations on Unstructured Meshes, AIAA Paper 97-2103, 13th AIAA CFD Conference, June, 1997.

[5] Smagorinsky, J., 1963, "General Circulation Experiments with the Primitive Equations, part I : The Basic Experiment," *Monthly Weather Review*, Vol. 91, pp.99.

[6] Lilly, D.K., 1992, "A Proposed Modification of the Germano Subgrid Scale Closure Method," *Physics of Fluids A*, Vol. 4, pp. 633-635.

[7] Kim, W.-W. and Menon, S., "Application of the Localized Dynamic Subgrid-Scale Model to Turbulent Wall-Bounded Flows, ", AIAA Paper 97-0210, presented at 35th Aerospace Sciences Meeting Exhibit, Reno, NV, January 6 - 10, 1997.

[8] Holmes, D.G. and Connel, S.D., 1989, "Solution of the 2D Navier-Stokes Equations on Unstructured Adaptive Grids," 89-1932-CP, Presented at the AIAA 9th Computational Fluid Dynamics Conference, June, 1989.

[9] Rauch, R.D., Batina, J.T., and Yang, H.T.Y., "Spatial Adaptation Procedures on Unstructured Meshes for Accurate Unsteady Aerodynamic Flow Computation," AIAA-91-1106, 1991.

[10] Frink, N.T., "Recent Progress Toward a Three-Dimensional Unstructured Navier-Stokes Flow Solver," AIAA-94-0061, 1994.

[11] jawahar, P. and Kamath, H.,"A High Resolution Procedure for Euler and Navier-Stokes Computations on Unstructured Grids", *J. Comput. Phys.* **164**, pp. 165 – 123, 2000.

[12] Bardina, J., Ferziger, J. H., and Reynolds, W. C., 1984, "Improved Turbulence Models Based on LES of Homogeneous Incompressible Turbulent Flows, Rep. TF-19, Department of Mechanical Engineering, Stanford.

[13] Clark, R. A., Ferziger, J. H. and Reynolds, W. C., 1979, Evaluation of Subgrid-Scale Models Using an Accurately Simulated Turbulent Flow, *J. Fluid Mech.*, **91**, pp. – 16.

[14] Germano, M., Piomelli, u., Moin, P., and Cabot, W.H., 1990, "Dynamic Subgrid Scale Eddy Viscosity Model," *Proc. Summer Workshop*, Center for Turbulence Research, Stanford CA.

[15] Ghosal, S., Lund, T., Moin, P., and Akselvoll, K., 1995, "A Dynamic Localization Model for Large Eddy Simulation of Turbulent Flows," *J. Fluid Mech.*, **286**, pp.29 – 255.

[16] Ghosal, S., Lund, T., Moin, P., and Akselvoll, K., 1995, Corrigendum, *J. Fluid Mech.*, **297**, pp.02 –.

[17] Kim, J. and Moin, P., 1985, "Application of Fractional Step Method to Incompressible Navier-Stokes Equations," *Journal of Computational Physics*, Vol. 59, pp. 308–323.

[18] Liu, S., Meneveau, C. and Katz, J., "On the Properties of Similarity SUbgrod-Scale Models as Deduced from Measurements in a Turbulent Jet,", *J. Fluid Mech.*, Vol. 275, pp. 83 – 119, 1994.

[19] Liu, S., Meneveau, C. and Katz, J., "Experimental Study of Similarity Subgrid-Scale Models of Turbulence in the Far-Field of a Jet, *Direct and Large Eddy Simulation I*, pp. 37 – 48, Kluwer, 1994.

[20] Moin, P. and Kim, J., 1982, "Numerical Investigation of Turbulent Channel Flow," *Journal of Fluid Mechanics*, Vol. 118, pp. 335–346.

[21] Piomelli, U. and Liu, J., 1995, "Large Eddy Simulation of Rotating Channel Flows Using a Localized Dynamic Model," *Phys. Fluids*, **7**(4), pp.39 – 847.

[22] Rai, M.M.. and Moin, P., 1991, "Direct Simulations of Turbulent Flow Using Finite-Difference Schemes," *Journal of Computational Physics*, Vol. 96, pp. 15–53.

[23] Rodi, W., Ferziger, J. H., Breuer, M., and Pourquie, M., "Status of Large Eddy Simulation: Results of a Workshop,", *Journal of Fluids Engineering*, Vol. 119, pp. 248 – 261, JUne 1997.

[24] Sohankar, A., Davidson, L., and Norberg, C., "Large Eddy Simulation of Flow Past a Square Cylinder: Comparison of Different Subgrid Scale Models," *Journal of Fluids Engineering*, Vol. 122, No. 1, pp. 376–404, March 2000.

[25] Lyn, D. A., Einav, S., Rodi, W., and Park, J. H., "A Laser Doppler Velocitimetry Study of the Ensemble-Averaged Characteristics of the Turbulent Near-Wake of a Square Cylinder," J. Fluid Mech., **304**, pp. 285 – 319, 1995.

[26] Wong, V. C., "A Proposed Statistical-Dynamic Closure Method for the Linear and Non-Linear Subgrid-Scale Stresses," *Phys. Fluids A*, **4**, pp. 1080 – 11082, 1992.

[27] Zang, Y., Street, R. L. and Koseff, J., 1993, "A dynamic Mixed Subgrid-Scale Model and its Application to Turbulent Recirculating Flows, *Phys. Fluids* A 5, pp.186